

Terrestrial Planet Finder Coronagraph optical modeling

Scott A. Basinger*, David C. Redding
Jet Propulsion Laboratory, California Institute of Technology
M/S 306-451, 4800 Oak Grove Drive, Pasadena, CA USA 91109-8099

ABSTRACT

The Terrestrial Planet Finder Coronagraph will rely heavily on modeling and analysis throughout its mission lifecycle. Optical modeling is especially important, since the tolerances on the optics as well as scattered light suppression are critical for the mission's success. The high contrast imaging necessary to observe a planet orbiting a distant star requires new and innovative technologies to be developed and tested, and detailed optical modeling provides predictions for evaluating design decisions. It also provides a means to develop and test algorithms designed to actively suppress scattered light via deformable mirrors and other techniques. The optical models are used in conjunction with structural and thermal models to create fully integrated optical/structural/thermal models that are used to evaluate dynamic effects of disturbances on the overall performance of the coronagraph. The optical models we have developed have been verified on the High Contrast Imaging Testbed. Results of the optical modeling verification and the methods used to perform full three-dimensional near-field diffraction analysis are presented.

Keywords: Terrestrial Planet Finder, coronagraph, modeling, optics, space telescopes

1. INTRODUCTION

The Terrestrial Planet Finder (TPF) Coronagraph has been well documented at the SPIE Europe International Symposium Astronomical Telescopes Conference that was held in Glasgow, Scotland, June 21-25 2004 [1-3]. The design for the TPF Coronagraph that is analyzed in the paper is called the "minimum mission design," and is documented in reference [2] and [4]. The design specifies a monolithic, elliptical primary mirror that is 6.0 m long and 3.5 m wide. Figure 1 shows a ray trace of the optical design.

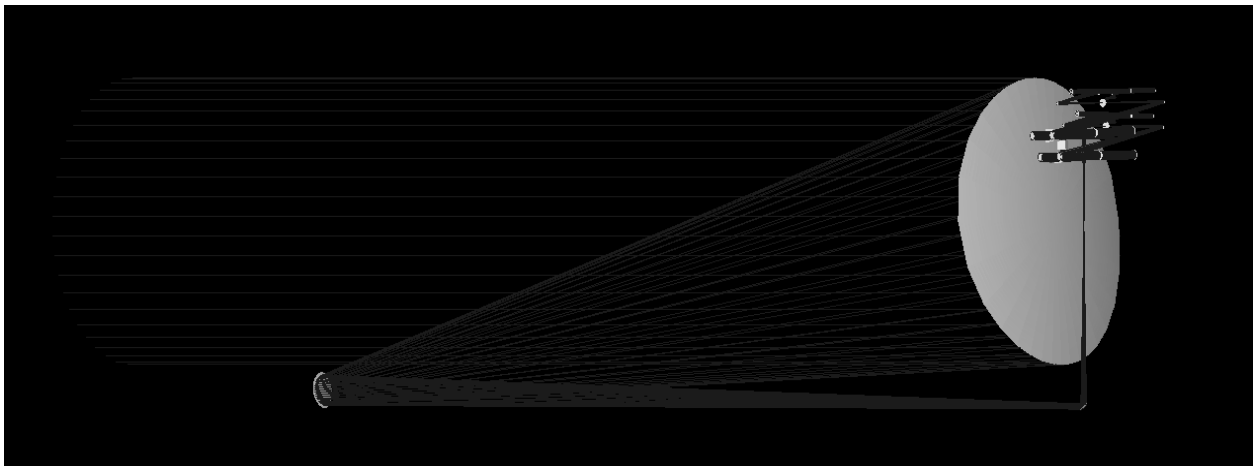


Fig.1. TPF Coronagraph minimum mission optical design

* Scott.A.Basinger@jpl.nasa.gov; phone 1 818 354-3065

This paper describes the optical modeling and analysis that has been performed for the TPF Coronagraph. Optical modeling is a subset of integrated modeling, which combines thermal, structural, and optical models to evaluate the performance of the design and allows for feedback to the design process. Integrated modeling enables insight into whether or not the requirements for the instrument are met when thermal and structural perturbations are applied to the system. Typical optical metrics, such as wavefront error and strehl ratio, are not adequate for evaluating the performance of a coronagraph. The ultimate metric is the contrast ratio for the instrument, and this can only be computed using diffraction models. Therefore, the second half of this paper describes the diffraction modeling process.

2. OPTICAL MODELING DESCRIPTION

2.1 Model Overview

The optical model is analyzed using MACOS (Modeling and Analysis for Controlled Optical Systems) [5], a tool developed and used by JPL/NASA for many projects. MACOS combines ray tracing and near-field scalar diffraction models in one tool. It allows seamless interfacing with structural models. We use The MathWorks MATLAB® as a front end for the optical model, which allows us to easily connect it to the thermal and structural models, which also interface to MATLAB.

The near-field diffraction capabilities built into MACOS have been developed to include routines that are optimized for various optical configurations. This includes diffraction propagation to optics that are neither at an image plane or a pupil plane. The diffraction routines use a propagation algorithm based on the Sziklas/Siegman form of the paraxial wave equation [6] and the computation is performed using the angular spectrum method [7]. Each optic has an apodized aperture applied to it so that diffraction effects are realistically captured in the model.

The prescription for the optical model is taken directly from the Zemax optical design. We have written a C program that converts the optical design from the local coordinate system that Zeemax uses into a global coordinate system that MACOS uses.

2.2 Model Topology and Characteristics

The centers of all the optics are listed in the spreadsheet below. The units are millimeters. “DOF” refers to the degrees-of-freedom associated with each optic. The row containing “offset” is used to globally translate the coordinates of each optic so that the center of the coordinate system of the optical model matches that of the structural model.

2.3 Modeling techniques and assumptions

Drift error: Drift error, or relative motion of individual optics, was not incorporated in the model. It is assumed that the optics are in the nominal alignment as specified by the optical design. Tolerance analysis is done by moving the optics relative to their nominal positions.

Coatings: No coatings were used in the optical modeling process described in this paper.

Wavelengths: The wavelength used in the optical model is 632.8 nm. This was chosen for the same reason it was chosen as the nominal wavelength in the optical design: optical testing will most likely be done at this wavelength. All simulations are monochromatic.

Masks & throughput: The occulting mask used in this analysis is a radial sinc^2 mask. The first “zero” of the sinc function is at the $4 \lambda/D$ point. The area of the Lyot stop that allows light to pass through was 31.82% of the total area of the pupil.

2.4 Model verification checks

The optical models were verified with early results on the High Contrast Imaging Testbed (HCIT) [3].

ele.	DOF	description offset	x	y	z
				0	0
					-12000
1	1-6	Primary	0.000000	0.000000	481.526650
2	7-12	Secondary	0.000000	-2060.158632	-9411.205470
3	13-18	Fold 1	0.000000	-2257.695358	893.200080
4	19-24	Fold 2	0.000000	1052.061486	899.078790
5	25-30	DM Collimator	897.679488	1056.119136	960.169650
6	31-36	Polarizing Beam Splitter 1 (3 surfaces)	-974.921862	1056.197096	960.164390
7	37-42	Polarizing Beam Splitter 2 (3 surfaces)	-974.904284	927.532868	968.710260
8	43-48	Steering Mirror	-975.067740	775.188251	978.828970
9	49-54	Michelson BS (3 surfaces, double pass)	-1136.249737	774.065796	978.903510
10	55-60	Wedge 1 (2 surfaces, double pass)	-1136.281686	769.076833	903.794120
11	61-66	DM 1	-1136.006418	764.777059	839.028630
12	67-72	Fold 3	-1136.249758	787.618481	1182.946800
13	73-78	Relay OAP 1	-2516.757556	780.560484	1222.062640
14	79-84	Relay OAP 2	481.518150	811.796270	1409.084590
		Pupil Mask	-837.246471	802.001493	1400.507720
15	85-90	Occulting OAP 1	-2274.422127	791.327249	1391.160730
16	91-96	Fold 4	1718.512615	1150.788568	1339.205150
17	97-102	Occulting Mask	-282.337001	1161.343931	1296.535180

Table 1. Optical elements through occulting mask.

3. OPTO-MECHANICAL SENSITIVITY ANALYSIS

3.1 Developing sensitivity matrices to WFE

Optical sensitivity matrices are developed using the MACOS model that is described above. A sensitivity matrix is a linear transformation that maps perturbations of the optics to wavefront error. In the case of a coronagraph, the contrast ratio is highly sensitive to the wavefront error at the exit pupil of the occulting mask. Therefore, the sensitivity matrices that we derived for this report are with respect to the wavefront at the exit pupil of the occulting mask.

There are many perturbations that can be explored. For this study, we examined rigid body perturbations of each optic individually in the optical beam path. Since the primary mirror is much larger than the other optics, we also studied the effect of allowing the primary mirror to be subdivided into a regular grid with 423 nodes evenly spaced on its surface.

The rigid body sensitivities are computed as follows: Each optical component is perturbed in all six degrees of freedom, one at a time. Each resulting wavefront at the exit pupil of the occulting mask is stored into a large matrix. The result is a linear "C-matrix" that can be multiplied by a vector of disturbances to reproduce a fully synthesized wavefront (see Fig. 3.1). It is assumed that all perturbations are small so that the small angle approximation is not violated and linearity can be assumed..

The rigid body perturbations are exercised in the global coordinate system, where the z-axis is the direction the light travels from the star to the primary mirror. This corresponds to the optical design and the structural and thermal models. The six degrees of freedom are: x-rotation, y-rotation, z-rotation, x-translation, y-translation, and z-translation. Rotations are performed about the named axis. The rotation point of each optic was chosen to be the place where the "gut ray," or the principle ray of the center field, intersects the optic. In the case of compound optics, such as a cube beam splitter, the rotation point was chosen in the center of the optic.

The mid-fidelity model has 423 equally-spaced nodes mapped on the primary mirror. To compute the sensitivities of the primary mirror flexible modes, each of the nodes was actuated by a small amount, one at a time, in the z-direction.

The resulting wavefront for each perturbation was calculated using MACOS and recorded as a vector in a matrix. In this way, a sensitivity matrix was computed for the wavefront error associated with allowing each node of the primary mirror to act as an “influence function.” This sensitivity matrix was validated by perturbing each node by a unit amount, at the same time, and comparing the resultant wavefront produced by perturbing the mirror using the rigid body sensitivity matrix by a unit amount in the z-direction. Both matched identically.

$$\begin{bmatrix} \text{DOF \#1 wavefront} \\ \text{DOF \#2 wavefront} \\ \vdots \\ \text{DOF \#96 wavefront} \end{bmatrix} \times \begin{bmatrix} \text{96 perturbations} \end{bmatrix} = \text{aberrated wavefront}$$

Fig. 3.1. Sensitivity matrix formulation.

3.2 Developing contrast results from the sensitivity analysis

The contrast ratio for wavefronts computed using the sensitivity matrices above can be computed from the error budget by decomposing the wavefronts into the first 15 Zernike terms and looking up the individual contribution to the contrast from the coefficient of each Zernike term. It has been verified that the wavefront errors caused by deformations on the primary are well represented by the first 15 Zernikes coefficients.

4. DIFFRACTION MODELING

Figure 4.1 shows intensity plots at various locations throughout the coronagraph. The first plot shows the point spread function (psf) just before the occulting mask. It is elliptical in shape because the primary mirror is elliptical. This particular plot is shown with a log stretch so that the airy rings can be seen, however, the rest in this sequence are plotted on a linear stretch. The second image shows the occulting mask. It is a radial sinc² function (1-sinc²), the first zero of which has been placed at the 4th airy ring of the psf to optimize the contrast at 3λ/D and the overall throughput through the coronagraph [8]. The third plot shows the intensity just after the occulting mask. The power in the central lobe has been drastically reduced so that the airy rings can be easily observed on a linear stretch. The fourth plot shows the intensity at the Lyot plane, before the aperture is applied. This is a pupil plane. The main feature is a bright ring, which is caused by high spatial frequencies in the image plane. We filter these high frequencies by applying an elliptical aperture. The resulting intensity is shown in the fifth plot. The sixth plot shows the psf at the final image plane. It is called a “speckle pattern” due to the random specks of light caused by residual scattering that is not corrected by the deformable mirrors in the optical system. Notice that the starlight has been suppressed so that it does not create a spike in the center of the plot. The residual speckles have more power than the central peak.

Figure 4.2 shows two examples of the aberrations applied to the surfaces of each optic in the coronagraph. The first plot shows the aberrations applied to the primary mirror and the second plot the secondary mirror. The mirror surfaces are randomly generated based on power spectral densities (psd’s) that are defined in our error budget for each optic.

Figure 4.3 shows the amplitude and phase of the electromagnetic field at the exit pupil of the occulting mask. The exit pupil of the occulting mask is the location at which it is critical to have an aberration-free wavefront. This simulation does not include a wavefront sensing and control algorithm, therefore, we ideally correct both the amplitude and phase errors at this location. Noise is added to the corrections so that the final contrast measurement is approximately 10⁻¹⁰. Figure 4.4 shows the corrected amplitude and phase at the exit pupil of the occulting mask. The amplitude has a large DC term, and therefore the noise is not visible. However, the noise can be seen in the phase measurement.

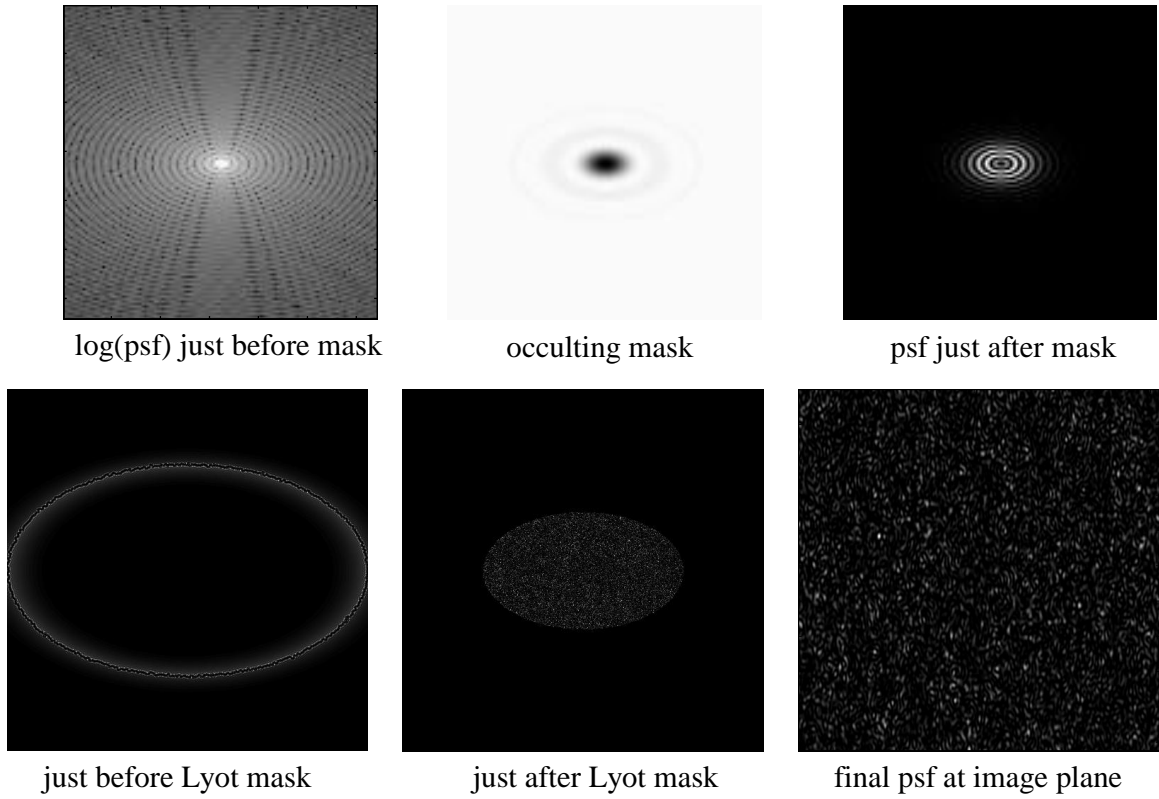


Fig. 4.1. Intensity plots at various locations throughout the coronagraph.

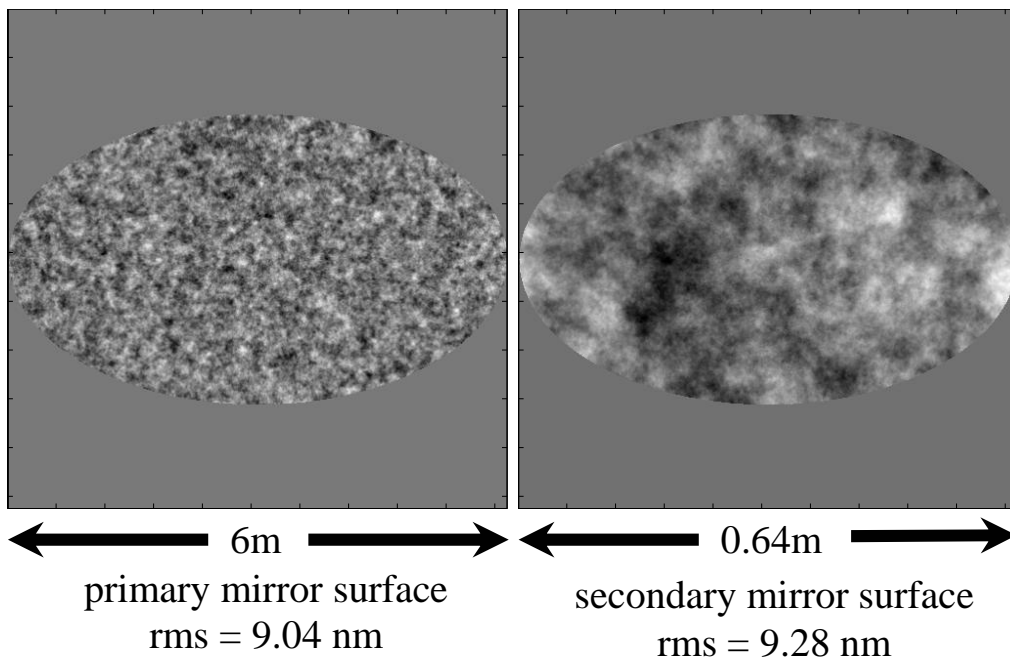


Fig. 4.2. Examples of randomly generated aberrations on optical surfaces.

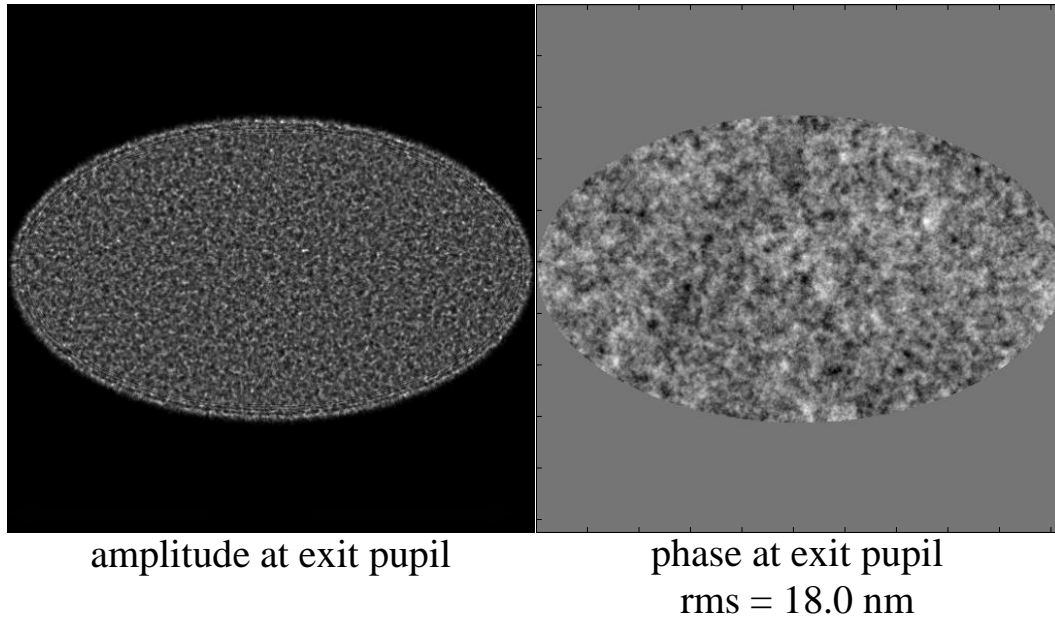


Fig. 4.3. Amplitude and phase at the exit pupil to the occulting mask.

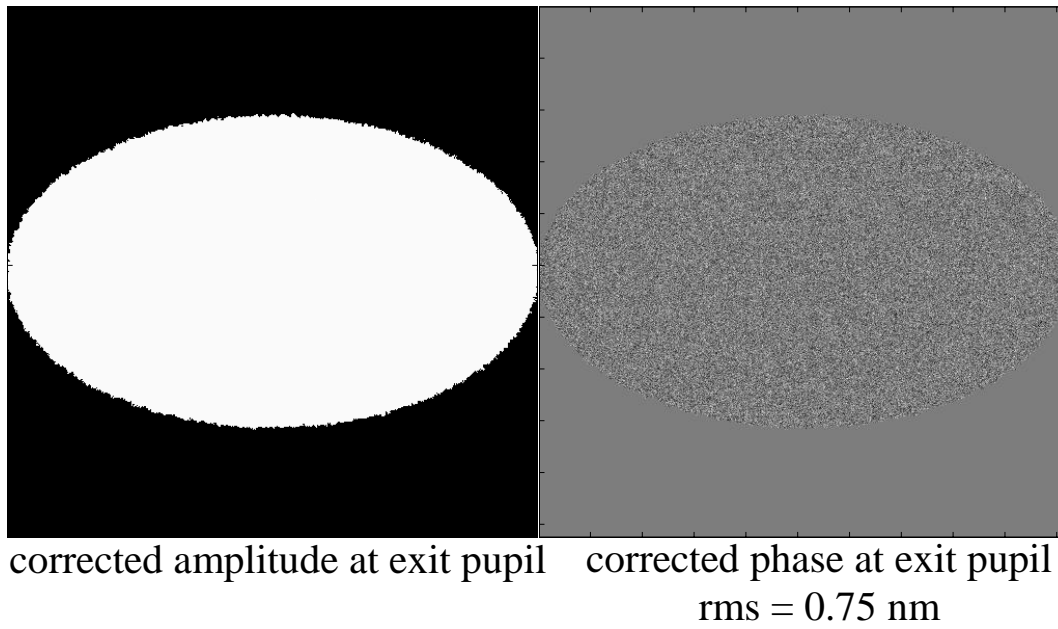


Fig. 4.4. Corrected amplitude and phase at the exit pupil to the occulting mask.

Figure 4.5. shows the azimuthally averaged contrast that is obtained with the coronagraph with all of the aberrations applied to the optics and the correction applied at the exit pupil of the occulting mask. The plot shows that the average contrast starting at $3\lambda/D$ is 10^{-10} .

Figure 4.6 shows a simulation of planet detection through the coronagraph. A planet was simulated along with a star with a relative intensity of 10^{-10} and a separation of $3\lambda/D$. Shot noise was included in the simulation and a read noise of 3 electrons was assumed. The first image shows the speckle pattern that is created. The planet's signal is washed out by the speckles. In the second image, the spacecraft is rotated by 20° . The speckles move along with the spacecraft, but the planet's signal does not. The third image shows the difference of the first two images, in which the location of the planet is clearly visible.

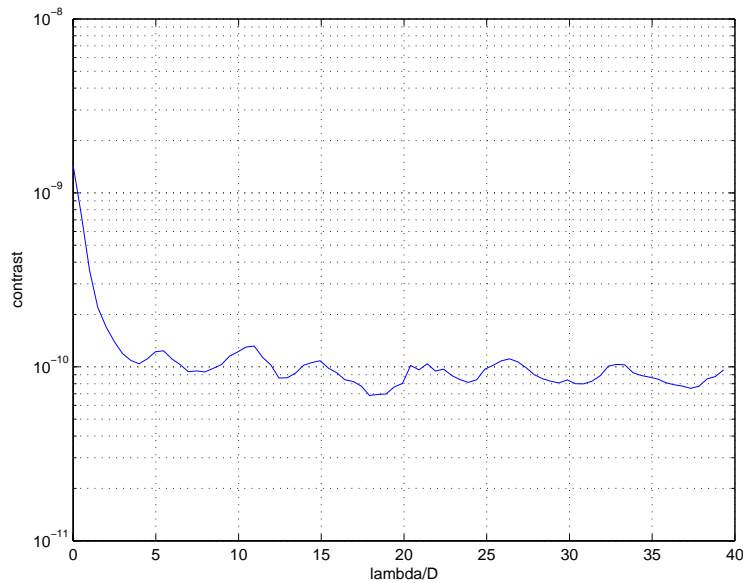


Fig. 4.5. Azimuthally averaged contrast.

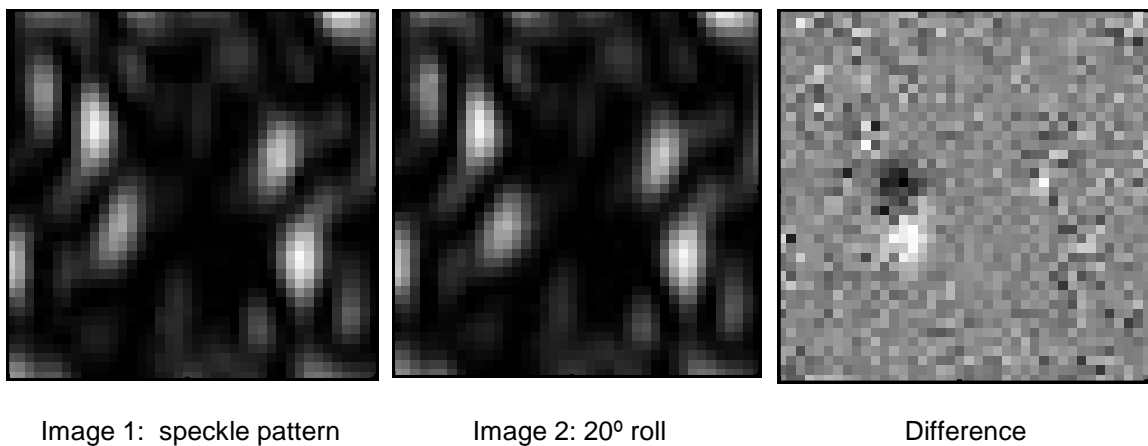


Fig. 4.6. Planet detection simulation.

5 SYNTHESIS OF INTEGRATED MODELING AND DIFFRACTION MODELING

Integrated modeling and diffraction modeling can be combined to provide full, end-to-end simulations of the behavior of the TPF Coronagraph for given disturbances. This is a very useful tool for examining whether the contrast levels can be maintained under various conditions. For example, one preliminary results that was computed was to determine the change in the contrast ratio for a 20° roll of the spacecraft. The 20° roll was chosen as a method for detecting a planet, as described in the above section and in Fig. 4.6. The wavefront sensing and control mechanism will not be reset during this maneuver, so it is important that the instrument is stable enough to withstand the thermal changes caused by the roll.

Figure 5.1 shows the change in contrast at $3\lambda/D$ over a 24 hour period after the spacecraft has been rolled by 20°. The main disturbance is caused by the change in the direction of the incident light from the Sun. Although there is a sunshield protecting the instrument, asymmetries still cause the temperature to affect the shape of the primary mirror and therefore the contrast ratio will change since the change in shape of the primary mirror is uncompensated after this maneuver by the wavefront sensing and control system. The steady-state change in contrast is about 0.95×10^{-11} .

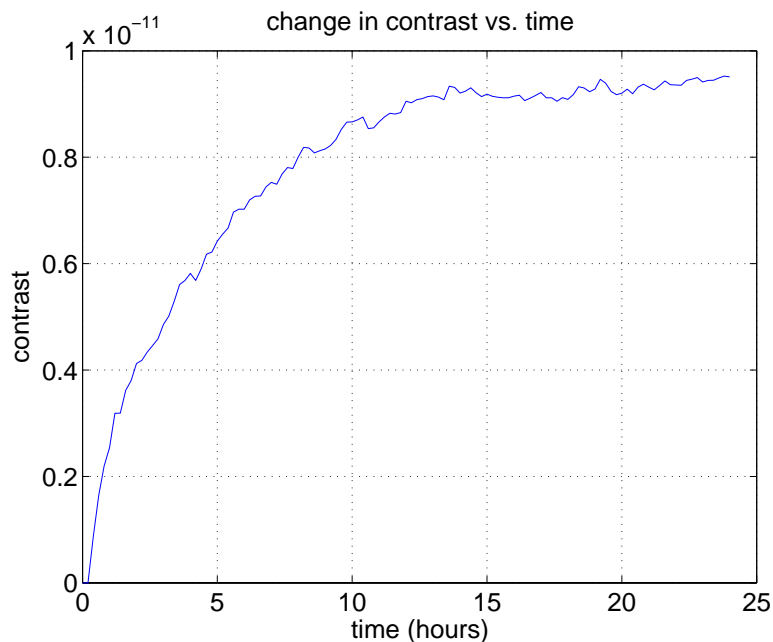


Fig. 5.1. Change in contrast at $3\lambda/D$ for a 20° roll.

ACKNOWLEDGMENTS

The research described in this paper was carried out at the Jet Propulsion Laboratory, California Institute of Technology, under a contract with the National Aeronautics and Space Administration.

REFERENCES

1. V. G. Ford, *The Terrestrial Planet Finder Coronagraph: Technology and Mission Design Studies*, SPIE Astronomical Telescope and Instrumentation Conf., Glasgow Scotland, June 2004. Paper [5487-182]
2. M. L. White, *Design and Performance of the Terrestrial Planet Finder Coronagraph*, SPIE Astronomical Telescope and Instrumentation Conf., Glasgow Scotland, June 2004. Paper [5487-59]
3. A. E. Lowman, et al., *High-Contrast Imaging Testbed For The Terrestrial Planet Finder Coronagraph*, SPIE Astronomical Telescope and Instrumentation Conf., Glasgow Scotland, June 2004. Paper [5487-178]
4. M. Levine et al., *Terrestrial Planet Finder Coronagraph – Minimum Mission Baseline Design and Analysis*, Jet Propulsion Laboratory, Pasadena CA, Report JPL D-28535, April 28, 2004.
5. *Modeling and Analysis for Controlled Optical Systems User's Manual*, Jet Propulsion Laboratory, California Institute of Technology, Pasadena CA.
6. Sziklas and Siegman, *Mode calculations in unstable resonators with flowing saturable gain2: Fast Fourier Transform method*, Applied Optics, v14, p. 1874-1889, 1975.
7. Siegman, *Lasers*, University Science Books, Mill Valley, CA, 1986.
8. J. J. Green, S. B. Shaklan, *Optimizing coronagraph designs to minimize their contrast sensitivity to low-order optical aberrations*, Proc. of SPIE Vol. 5170.